

Short Communication

Characterization of MnCo_2O_4 as anode material for a Sodium-Air Electric Vehicle Battery

Han Peng*

School of Mechanical Engineering, North China University of Water Resources and Hydropower, Dengzhou City, Henan Province, 450045, P.R. China

*E-mail: 727787302@qq.com

Received: 7 December 2017 / Accepted: 29 January 2018 / Published: 6 March 2018

Among multiple next-generation rechargeable energy storage systems (e.g., electric vehicle battery), one substitution for lithium-ion batteries (LIBs) is the sodium-ion battery (SIBs). However, the thermodynamic and kinetic properties of SIBs remain uncertain, considering the distinct (de)sodiation processes and larger ionic radius of the sodium cation. The present work demonstrates the fabrication of inorganic MnCo_2O_4 nanoparticle-based SIBs. Under dry air experimental conditions, the $\text{MnCo}_2\text{O}_4/\text{C}$ -air electrode showed a high initial discharge capacity (7502 mA/h/g) and a stable working voltage (~ 2.1 V against Na^+/Na).

Keywords: Sodium-air batteries; MnCo_2O_4 ; Electric vehicle battery; Charge-discharge

1. INTRODUCTION

Hybrid vehicles and electric vehicles have been gaining increasing popularity in the market, which is predicted to continue in the future. There is widespread agreement that climate change is caused by humans [1, 2], as indicated in the legislation of point-of-use emissions domestically and overseas, especially since strict regulations have been introduced in Europe. Based on an estimation from the UK Government, average ‘new car’ tailpipe emissions must be reduced to ~ 50 – 70 g/km (approximately half of the present-day value) by 2030 [3-5]. It is a consensus in global academic fields that new and rapidly expanding markets (China, India, etc.) are strongly conscious of the necessity for sustainable development and that it is unwise to depend too heavily on scarce foreign oil imports. For the newest generation of transport systems, applications of renewable energy sources have been previously reported, along with many different novel techniques [6-8]. It can be presumed that future

powertrain systems would be highly electrified, hybridized, and more dependent on affordable, effective, and high-quality traction batteries.

The electrification of vehicles mainly lies in the development of energy storage systems. For electric and hybrid vehicles, ultracapacitors, fuel cells, batteries, etc. have been enhanced by multiple techniques. Among these techniques, an extensively applied strategy in advanced electrified vehicles is the use of lithium ion (Li-ion) batteries. Additionally, Li-ion batteries have been designed with various chemical compositions to cater to corresponding specifications. Battery energy density, reliability, and safety are the main considerations during their use in automotive applications [9-11]. In EVs, common Li-ion batteries include lithium cobalt oxide (LCO), lithium nickel–manganese–cobalt oxide (NMC), lithium iron phosphate (LFP), and lithium manganese oxide (LMO) [12, 13].

However, the lithium-air cell suffers certain drawbacks, including a significantly low power of ~ 0.1 to 1 mA cm^{-2} as well as a high reactivity of lithium peroxide and lithium superoxide (oxygen-discharge products) to the electrolyte solvents and environment [14-16]. Additionally, considering their electrically insulating properties, solid peroxides require a carbon substrate with a large area, and the thickness of these solid peroxides must be lower than the tunneling range of electrons. Briefly, the thickness of a lithium peroxide layer on the carbon matrix must be lower than $\sim 25 \text{ \AA}$. Generally, side reactions based on the electrocatalyst employed in the air electrode show high sensitivity toward the atmosphere. The air moisture effect on the electrochemical performance of the sodium-air batteries has been extensively reported. To prevent unpredictable and undesirable side reactions, oxygen has been used to substitute air as the test atmosphere [17]. Therefore, sodium-air batteries have advantages over sodium-oxygen batteries in view of practicability [18-20].

The present study reports the synthesis of MnCo_2O_4 , and its utility as an excellent catalyst for sodium-air batteries was also investigated. The sodium-air battery sheds some insight into the development of novel high-specific-energy rechargeable batteries.

2. EXPERIMENTS

2.1. MnCo_2O_4 Synthesis and characterization

The synthesis of MnCo_2O_4 microspheres was based on a hydrothermal method by dissolving $\text{MnCl}_2 \cdot 4\text{H}_2\text{O}$ (1 mM) and $\text{CoCl}_2 \cdot 6\text{H}_2\text{O}$ (2 mM) of a certain amount into a mixed solution containing ethylene glycol and deionized water (volume ratio: 4:1). Then, the as-prepared mixture was further added with hexadecyl trimethyl ammonium bromide (CTAB; 0.01 mM) to obtain the required sphere morphology. After thorough dissolution, this mixture was subsequently added with NH_4HCO_3 at a molar ratio of HCO_3^- vs. $(\text{Mn}^{2+} + \text{Co}^{2+})$ of 2.4:1 and vigorously stirred to yield a homogeneous mixture. The obtained homogeneous solution was stirred for 30 min before being transferred into a 100 mL flask. In addition, a hydrothermal reaction was carried out for 300 min at $120 \text{ }^\circ\text{C}$. Then, the reaction was cooled to ambient temperature in an autoclave, and the product was centrifuged to yield the precipitate, followed by washing and drying in vacuum. The final product in the form of dried

powder was calcined in air for 120 min at 500 °C. An X-ray diffractometer (Rigaku, Ultima IV, Japan) with Cu K α radiation ($\lambda=1.5418$ Å) was used to study the phase purity and crystallinity of the product.

2.2. Electrochemical measurements

The test electrode was prepared by mixing the as-prepared MnCo₂O₄ with polyvinylidene fluoride and carbon black (85:7.5:7.5) in *N*-methylpyrrolidinone, and the last 7.5 refers to the sum of the coated carbon and the added carbon black, accounting for 3.7 and 3.8 (wt%) for the carbon-coated MnCo₂O₄ electrode, respectively. Then, the Cu foil was modified by the produced slurries, followed by roll-pressing. Super P carbon paste electrode was prepared using Super P (Alfa Aesar) black with similar fabrication process without adding MnCo₂O₄. Before testing, these electrodes left to dry in a vacuum at 80 °C overnight. We carried out the charge-discharge experiments with R2032-type coin cells with a counter electrode of Na metal. To prepare the test electrolyte, NaClO₄ (1 M) was added into a mixed solution of polycarbonate and fluoroethylene carbonate at a volume ratio of 98:2. The cycling of cells was performed at 25 °C over a voltage range from 0.7 V to 2.7 V (35 mA/g (0.2 C) to 17.5 A/g). Another method of significantly decreasing irreversible capacity has been proposed herein, i.e., pre-sodiation. For pre-sodiation, extra capacity from the formation of a solid–electrolyte interface (SEI) and the reductive decomposition of electrolyte were eliminated by keeping the carbon-coated MnCo₂O₄ electrode in direct contact with the Na metal in the electrolyte. The whole process was carried out in an Ar-filled glove box. The open circuit voltage (OCV) of the carbon-coated MnCo₂O₄ electrode during pre-sodiation was continuously monitored. After 20 min, the anode reached ~ 0.82 V vs. Na/Na⁺, corresponding to an initial voltage that accommodates Na⁺ ions in the spinel structure. Subsequently, the pre-sodiation process was finished.

3. RESULTS AND DISCUSSION

The typical XRD patterns of the MnCo₂O₄ powders prepared at a hydrothermal reaction temperature of 160 °C are shown in Figure 1. All the diffraction peaks correspond well to the cubic phase of MnCo₂O₄. These characterizations exhibit no significant peaks corresponding to the impurity phase. All the diffraction peaks can be indexed as the pure spinel structure phase of space group Fd3m MnCo₂O₄ (PDF number: 23-1237). No additional peaks for other phases such as CoO or MnO₂, were observed [21]. Therefore, MnCo₂O₄ is a mixed valence oxide with a cubic spinel structure, where the cobalt and manganese are distributed over both tetrahedral and octahedral sites. It had been proposed that the as-prepared compound is structurally stable and, meanwhile, could provide a large quantity of active sites for the oxygen evolution reaction (OER) as well as the oxygen reduction reaction (ORR) [22, 23]. The cell parameter obtained from the Rietveld refinement with a convincing R_{wp} value is $a = 8.322$ Å.

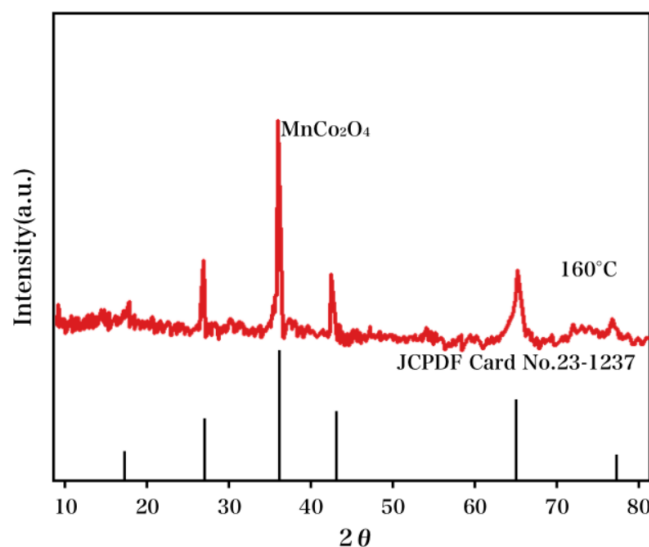


Figure 1. XRD pattern recorded for the obtained MnCo₂O₄ microspheres. Inset: the crystal structure model.

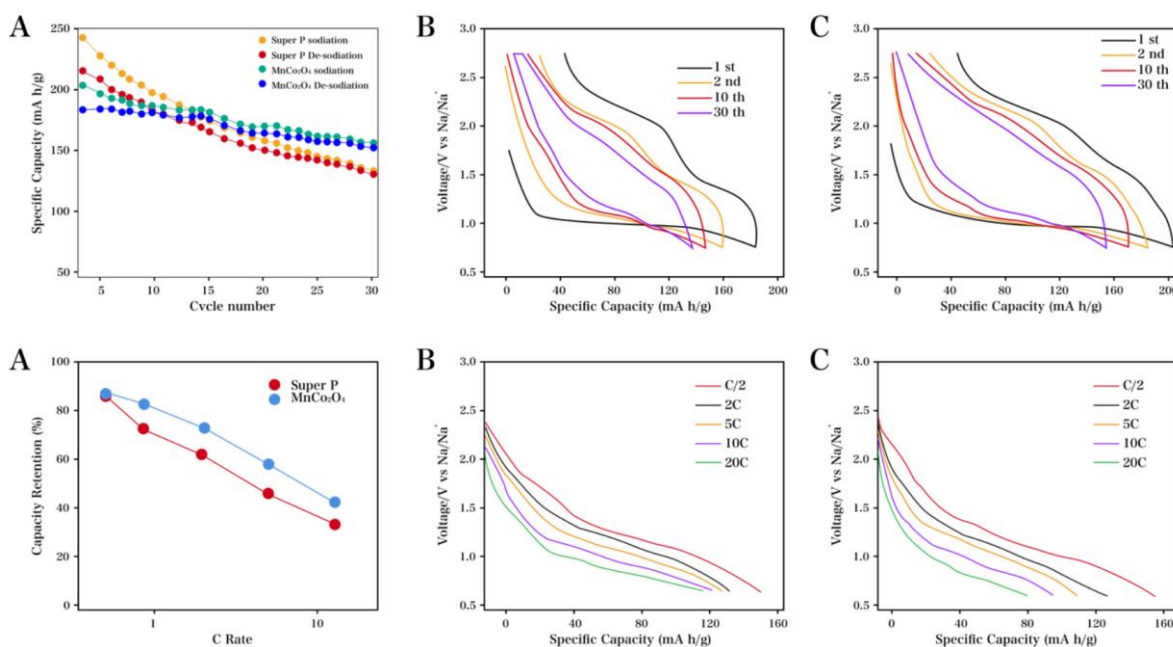


Figure 2. (A) Cycle performance of Super P and MnCo₂O₄ at a current density of 20 mA/g (0.1 C) and their corresponding voltage patterns recorded for (B) MnCo₂O₄ and (C) Super P; (D) Rate performance of Super P and MnCo₂O₄, and their corresponding voltage patterns recorded for (E) MnCo₂O₄ and (F) Super P.

Figure 2 shows the electrochemical behavior comparison between Super P (control) and MnCo₂O₄ electrodes. The cycling of cells was performed over a voltage range of 0.7 V to 2.7 V vs. Na/Na⁺. Compared with the control group, the MnCo₂O₄ electrode exhibited a much more desirable cycle behavior. As shown in Figure 2A, the control group and the MnCo₂O₄ electrode showed a capacity retention of 48% and 76% after 30 cycles, respectively. At each cycle run, both Super P and

the MnCo_2O_4 electrodes exhibited comparable voltage patterns; however, with the increase in cycle number, the former showed more polarization than the latter, as shown in Figure 2B and 2C. It has been reported that capacity of transition metal selenide for sodium-ion batteries could dramatically decrease [24]. A comparison of their rate performance is shown in Figure 3D-F. Compared with the control group, the MnCo_2O_4 electrode showed a more favorable rate performance and delivered approximately 74 mA/h/g (even at a rate of 20 C), which resulted from the larger number of defective channels and enhanced electrical conductivity of the as-prepared MnCo_2O_4 .

We studied the electrochemical characteristics of the MnCo_2O_4 electrode in sodium-air batteries, together with those of the Super P electrode. CVs were recorded for these two electrodes during the first cycle (scan rate: 1 mV/s; 1.5 to 4.0 V), as shown in Figure 3. During the ORR, the MnCo_2O_4 electrode showed a slightly larger cathodic current at the peak position of 2.1 V compared with that of the control group. The oxidation peaks were not as sharp as the reduction peaks, indicating that reaction causes the accumulation of MnCo_2O_4 [25, 26]. During the OER, the control group showed no significant cathodic peak, while the MnCo_2O_4 electrode exhibited an obviously increased current response at approximately 3.3 V, which suggested that the MnCo_2O_4 electrode showed more rapid OER kinetics and, correspondingly, an enhanced catalytic activity. For both the Super P-based and MnCo_2O_4 -based electrodes, the discharge-charge characterizations are shown in Figure 3 (current density: 0.1 mA/cm²; voltage: 1.5–4.0 V). Compared with the control group, the MnCo_2O_4 electrode exhibited an ~ 0.2 V higher discharge plateau, indicating a lower polarization. Additionally, the MnCo_2O_4 electrode shows a high initial discharge capacity (7502 mA/h/g) with a stable voltage output that is significantly higher than that of the control group (2007 mA/h/g). For the control group and the MnCo_2O_4 -based electrode, the initial coulombic efficiency was 80.6% and 87.7%, respectively, which suggests that the decomposition of the discharge products on the air electrode is effectively promoted by the MnCo_2O_4 microspheres. A desirable consistency has been found between the CV characterizations and the discharge and charge performance, which suggests distinct catalytic activity of the developed MnCo_2O_4 compared to that of the conventional Super P-based air electrode.

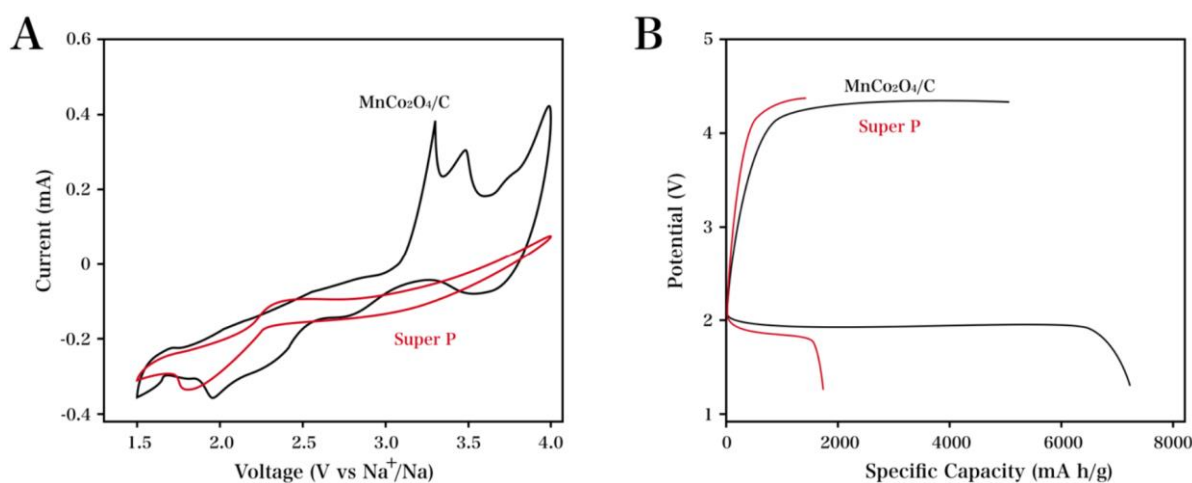


Figure 3. (A) CV curves recorded for the MnCo_2O_4 and Super P electrodes at the first cycle (scan rate: 1 mV/s) and (B) discharge-charge curves recorded for the MnCo_2O_4 and Super P electrodes at the first cycle (current density: 0.1 mA/cm²).

Figure 4 shows the electrochemical impedance spectroscopy (EIS) profiles of the cells, demonstrating their variation in resistance before and after the cycles. The cells were measured at their discharged stages to study the effects of the products on the air electrode. The first semicircle at a high frequency may result from the ohmic resistance, corresponding to the synergistic effects of the cathodic deposition, the formation of discharge products on the air electrode and the electrolyte resistance within the electrode material [27]. The charge-transfer resistance (R_{ct}) of the cell was found to sharply increase over a range from 81 Ω (obtained at the assembly stage) to 117 Ω (obtained after the first discharge cycle), which may result from the fact that a large numbers of discharge products aggregated on the air electrode surface [28]. As the cycle number increased, a gradual increase in the cell resistance was found. This may cause rapid capacity fading in the cell. The observation can greatly explain the result of the discharge-charge curves.

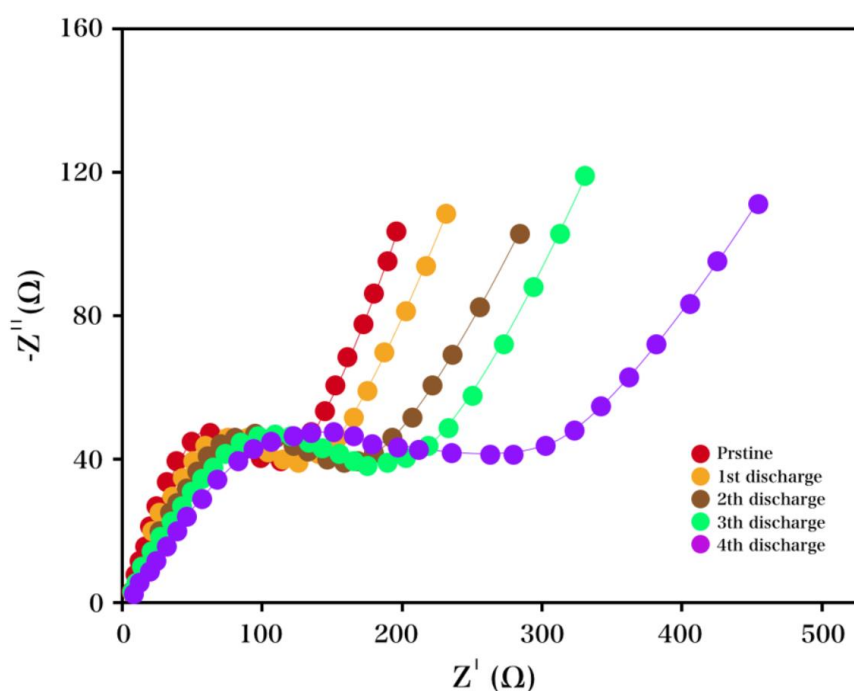
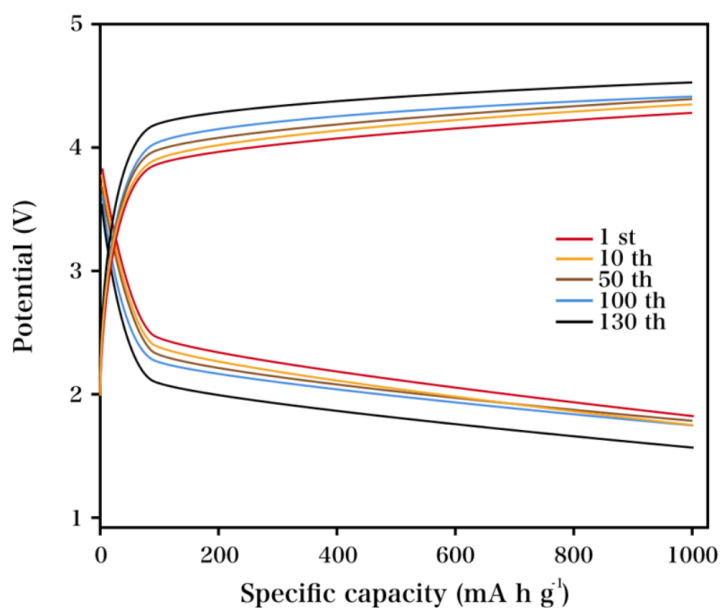


Figure 4. EIS results recorded for the MnCo_2O_4 electrode at the assembly stage and the fully discharged states during the initial 5 cycles.

Based on the literature, cycling the cell under a restricted depth of discharge (DOD) has been found to significantly enhance the cycling performance. Under a restricted DOD at a capacity cut-off of 1000 mA/h/g, the cell could be cycled up to 130 times, showing high reversibility. Additionally, the cycling stability was comparable to or even more favorable than that of sodium-air batteries based on varying cathode catalysts [29]. Figure 7 illustrates the discharge and charge profiles of the MnCo_2O_4 electrode. Unfortunately, as the cycle number increased, an increase in the voltage polarization during discharge and charge was also observed. The voltage gap between the discharge and charge was ~ 1.5 – 2.0 V, which suggests serious polarization. This may result from the resistance and electrochemical activity of the cell, which are greatly influenced by the products of the air electrode associated with the experimental conditions. Some similar anode materials are listed in Table 1 and are compared with the MnCo_2O_4 nanoparticles prepared in this work.

Table 1. Comparison between MnCo_2O_4 and similar anode materials in the literature.

Material	Charge-discharge current density (mA/g)	Charge-discharge End voltage	Initial discharge capacity (mAh/)	Initial charge capacity (mAh/g)	Reference
CoSe_2	50	2.5-0 V	975.9	516.9	[30]
NiSe_2	50	3.0-1.0 V	468.5	460.3	[31]
SnSe	50	3.0-0.01 V	1009.0	417.0	[32]
ZnSe	40	3.0-0.01V	960.0	530.0	[33]
MnCo_2O_4	50	2-4 V	1000.0	660.4	This work

**Figure 5.** Charge and discharge performance of the MnCo_2O_4 .

4. CONCLUSIONS

The present study proposed the synthesis of a novel MnCo_2O_4 catalyst using a hydrothermal method and demonstrated its application as an air electrode for sodium-air batteries. Due to the synergistic effect of a larger number of diffusion channels along the c axis and improved electrical conductivity, MnCo_2O_4 exhibited favorable cyclability and an enhanced rate performance over 130 cycles compared to Super P, suggesting desirable electrochemical performance. Despite the slow diffusion kinetics of MnCo_2O_4 , its electrochemical performance could be enhanced after the structural modification via doping, as proposed herein.

References

1. Z. Chen, A. Yu, D. Higgins, H. Li, H. Wang and Z. Chen, *Nano Letters*, 12 (2012) 1946.
2. W. Hardin, D. Slanac, X. Wang, S. Dai, K. Johnston and K. Stevenson, *Journal of Physical Chemistry Letters*, 4 (2013) 1254.
3. O. Crowther, D. Keeny, D. Moureau, B. Meyer, M. Salomon and M. Hendrickson, *Journal of Power Sources*, 202 (2012) 347.
4. H. Park, U. Dong, Y. Liu, J. Wu, L. Nazar and Z. Chen, *Journal of the Electrochemical Society*, 160 (2013) A2244.
5. H. Zhang, H. Qiao, H. Wang, N. Zhou, J. Chen, Y. Tang, J. Li and C. Huang, *Nanoscale*, 6 (2014) 10235.
6. J. Hu, Q. Liu, L. Shi, Z. Shi and H. Huang, *Appl. Surf. Sci.*, 402 (2017) 61.
7. S. Noh, C. Kwon, J. Hwang, T. Ohsaka, B. Kim, T. Kim, Y. Yoon, Z. Chen, M. Seo and B. Han, *Nanoscale*, 9 (2017)
8. M. Wang, T. Qian, J. Zhou and C. Yan, *ACS Applied Materials & Interfaces*, 9 (2017) 5213.
9. G. Abrenica, J. Ocon and J. Lee, *Current Applied Physics*, 16 (2016) 1075.
10. L. Otaegui, I. Laresgoiti, C. Bernuy-López, N. Gómez, M. Alvarez, L. Wang, T. Rojo and L. Rodriguez-Martinez, *Electrochimica Acta*, 214 (2016) 192.
11. J. Stuart, M. Leflerm, C. Rhodes and S. Licht, *Journal of the Electrochemical Society*, 162 (2015) A432.
12. S. Mohammadian, S. Rassoulinejad-Mousavi and Y. Zhang, *Journal of Power Sources*, 296 (2015) 305.
13. Z. Wang, D. Xu, J. Xu and X. Zhang, *Chemical Society Reviews*, 43 (2014) 7746.
14. S. Velraj and J. Zhu, *Journal of Electroanalytical Chemistry*, 736 (2015) 76.
15. L. Otaegui, L. Rodriguez-Martinez, L. Wang, A. Laresgoiti, H. Tsukamoto, M. Han, C. Tsai, I. Laresgoiti, C. López and T. Rojo, *Journal of Power Sources*, 247 (2014) 749.
16. A. Inoishi, H. Kim, T. Sakai, Y. Ju, S. Ida and T. Ishihara, *Chemosuschem*, 8 (2015) 1264.
17. J. Whiteley, J. Woo, E. Hu, K. Nam and S. Lee, *Journal of the Electrochemical Society*, 161 (2014) A1812.
18. D. Gelman, B. Shvartsev and Y. Ein-Eli, *Topics in Current Chemistry*, 374 (2016) 82.
19. M. Hilder, B. Winther-Jensen and N. Clark, *Electrochimica Acta*, 69 (2012) 308.
20. A. Ven, B. Puchala and T. Nagase, *Journal of Power Sources*, 242 (2013) 400.
21. H. Liu and J. Wang, *Journal of Electronic Materials*, 41 (2012) 3107.
22. E. Peled, D. Golodnitsky, H. Mazor, M. Goor and S. Avshalomov, *Journal of Power Sources*, 196 (2011) 6835.
23. P. Hartmann, C. Bender, J. Sann, A.K. Dürr, M. Jansen, J. Janek and P. Adelhelm, *Phys Chem Chem Phys*, 15 (2013) 11661.
24. W. Lu, M. Xue, X. Chen and C. Chen, *Int. J. Electrochem. Sci.*, 12 (2017) 1118.
25. Z. Zou, Q. Yuan, J. Wang, Y. Gao, Y. Wu, F. Long, S. Han and Z. Wan, *International Journal Of Electrochemical Science*, 12 (2017) 1670.
26. L. Fu, K. Xie, H. Zhang, Y. Zheng, W. Su and Z. Liu, *Coatings*, 7 (2017) 232.
27. M. Alaf, U. Tocoglu, M. Kartal and H. Akbulut, *Appl. Surf. Sci.*, 380 (2016) 185.
28. Y. Li, H. Yadegari, X. Li, M.N. Banis, R. Li and X. Sun, *Chemical Communications*, 49 (2013) 11731.
29. I. Bardenhagen, M. Fenske, D. Fenske, A. Wittstock and M. Bäumer, *Journal of Power Sources*, 299 (2015) 162.
30. M. Xue and Z. Fu, *Electrochemistry Communications*, 8 (2006) 1855.
31. N. Li, Y. Zhang, H. Zhao, Z. Liu, X. Zhang and Y. Du, *Inorganic Chemistry*, 55 (2016) 2765.
32. S. Kang, L. Jia, X. Li, Y. Yin, L. Li, Y. Guo and J. Mu, *Colloids and Surfaces A: Physicochemical and Engineering Aspects*, 406 (2012) 1.

33. Y. Fu, Z. Zhang, K. Du, Y. Qu, Q. Li and X. Yang, *Materials Letters*, 146 (2015) 96

© 2018 The Authors. Published by ESG (www.electrochemsci.org). This article is an open access article distributed under the terms and conditions of the Creative Commons Attribution license (<http://creativecommons.org/licenses/by/4.0/>).